

# X-Ray-Absorption Edge Separation Using Diffraction Anomalous Fine-Structure

B. Ravel\*, C. E. Bouldin\*, H. Renevier†, J.-L. Hodeau†, J.-F. Berar†

\*National Institute of Standards and Technology, Gaithersburg, MD 20899

†Laboratoire de Cristallographie, CNRS, BP 66, 38042 Grenoble Cedex 09 France

(December 24, 1998)

When two or more absorption edges in a material are sufficiently close in energy, Extended X-ray-Absorption Fine-Structure (EXAFS) spectroscopy is of limited utility as the usable data range above the lower energy edge is truncated by the higher energy edge. Energy or wavelength discriminating detection methods may fail to resolve fluorescence lines which are very close in energy. In this paper we present a novel solution to this problem using the resolution in momentum transfer of Diffraction Anomalous Fine-Structure (DAFS) to separate the fine structure signals from elements with closely spaced fluorescence lines. We demonstrate our technique by isolating the titanium edge signal from DAFS measurements of BaTiO<sub>3</sub>.

Materials containing atoms with absorption edges closely spaced in energy are a common challenge in the field of Extended X-ray-Absorption Fine-Structure (EXAFS). When a non-energy discriminating detection method, for example an ionization chamber [1], is used in any of the standard EXAFS measurement geometries [2], the presence of the higher energy edge places a hard limit on the energy range over which data from the lower energy edge can be measured. The edge step of the higher energy absorber is generally larger than the EXAFS oscillations from the lower energy absorber and there is no reliable a posteriori way of removing the higher energy edge step from the measurement. For some materials, the edges are sufficiently close that the data range from the lower edge is too limited to allow quantitative analysis. In these cases, the only recourse has been energy or wavelength discriminating detectors to reject the photons at the fluorescent energy of the higher edge-energy atom. When the energy separation of the fluorescent lines is sufficiently small these methods will fail.

Diffraction Anomalous Fine-Structure (DAFS) [3] combines the crystallographic sensitivity of diffraction with the short range order sensitivity of EXAFS. This has been used to isolate the signal from spatially distinct regions of a sample in a mixed powder [4] and in a multi-layer film [5]. DAFS can also separate the fine-structure signals of atoms in different sites of a crystal. For example, DAFS has been used to separate the fine structures of Cu sites in YBa<sub>2</sub>Cu<sub>3</sub>O<sub>7</sub> [6] or Fe sites in BaZnFe<sub>6</sub>O<sub>11</sub> [7]. In those works, DAFS was used to site-separate a single atomic species residing in multiple crystallographic sites. We extend this approach to consider the site-separation of *different* atomic species residing in *different* crystallographic sites. The DAFS method separates absorption edge signals using resolution of the photon momentum transfer vector  $\mathbf{Q}$  rather than resolution of the photon energy. Thus it can be used to separate the fine structure signal from atoms with arbitrarily closely spaced fluorescent lines, provided they reside in different crystallographic sites.

In this paper, we demonstrate our DAFS technique by isolating the Ti edge signal from measurements of BaTiO<sub>3</sub>. BaTiO<sub>3</sub> is an excellent candidate for this approach for several reasons. First, the Ti K edge is at 4966 eV while the Ba L<sub>III</sub> is at 5247 eV, as shown in Figure 1. The separation of 281 eV, or about 8.2 Å<sup>-1</sup> in photoelectron wave-number, places a severe restriction on the information content of the Ti K edge signal. In addition, the dominant fluorescent lines, the Ti K<sub>α<sub>1</sub></sub> and Ba L<sub>α<sub>1</sub></sub>, are separated by just 45 eV, less than the  $\mathcal{O}(10^2)$  eV resolution of most energy discriminating detectors. In fact, our attempt to separate the Ti K<sub>α<sub>1</sub></sub> and Ba L<sub>α<sub>1</sub></sub> lines using a Si(Li) detector failed. Finally, BaTiO<sub>3</sub> is a system that has been well-studied by EXAFS [8] at the Ba K edge and therefore previous results can be compared to the analysis of our site separated Ti  $\chi(k)$  data.

## I. THE DAFS MEASUREMENT

The intensity of a diffraction peak at momentum transfer  $\mathbf{Q}$  is given by

$$I(\mathbf{Q}) = \left| \sum_j F_j e^{i\mathbf{Q}\cdot\mathbf{R}_j} M_j \right|^2 \quad (1)$$

where the sum is over all sites  $j$  in the unit cell of the crystal,  $\mathbf{R}_j$  are the positions of the sites in the cell, and  $M_j$  are the thermal factors.  $F_j$  is the atomic scattering factor. Far away from any absorption edge this is the Thomson scattering  $f^0(\mathbf{Q})$ , which depends on the momentum transfer but not on the energy of the incident photon. Near the absorption of an atom, there is a complex, energy dependent correction to the scattering factor such that the  $F_j$  in Eq. (1) is expressed [3] as

$$F_j = f_j^0(\mathbf{Q}) + f_j'(E) + if_j''(E) + [\Delta f_j''(E) \cdot \chi_j(E)]. \quad (2)$$

The terms  $f'$  and  $f''$  are the atomic portion of the energy dependent anomalous correction and are analogous

to the anomalous dispersion observed in optical spectra. Because the virtual photoelectron excited in the diffraction process can scatter off of surrounding atoms, there is a fine structure term  $\chi_j$ .  $\chi_j$  is the coefficient of  $\Delta f_j''$ , the portion of  $f_j''$  due to the resonant electron. The imaginary part of  $\chi_j$  is the fine structure function measured in EXAFS.

In the DAFS experiment, the intensity of a particular diffraction peak is measured as a function of energy. This measurement requires a tunable energy source, such as the monochromator found on an EXAFS beamline at a synchrotron facility, and a way of tracking the peak position in reciprocal space as the energy is tuned through an energy range containing the resonant energies. The DAFS data reported in this paper were obtained at beamline BM2 [9] at the European Synchrotron Radiation Facility in Grenoble, France. BM2 is a bending magnet beamline with a double crystal silicon (111) monochromator with sagittal focusing. Mirrors are used to reject harmonic content and to focus the beam vertically. The sample sat at the center of a 7-circle goniometer and was mounted on the cold finger of a two-stage helium compressor cryostat. The incident intensity was measured with a scintillator using the scatter from a thin piece of kapton film. The diffracted intensity was measured with a PIN silicon diode in current mode.

The BaTiO<sub>3</sub> sample was a 1000 Å film deposited by pulsed laser deposition onto a sapphire substrate. The film was found by diffraction to be a highly oriented single crystal with a lattice constant in the vertical scattering plane of 4.0043(2) Å. For this experiment, we performed DAFS measurements on (*h*00) peaks, i.e. with momentum transfer in the vertical scattering plane. Once the sample was aligned in the goniometer and placed in the focal spot of the beamline optics, the positions of the (*h*00) peaks were tracked by the  $\theta$ - $2\theta$  motion of the goniometer as the energy was varied. Because of the long wavelength of the photons near the Ti K edge energy ( $\lambda \approx 2.5$  Å near the Ti K edge), the short lattice constant of BaTiO<sub>3</sub>, and the limited goniometer range only the first three (*h*00) peaks were measured. 3 scans of each reflection were collected at 130 K. Sample DAFS spectra for the (100) and (200) peaks are shown in Figure 2. The intensity of the (300) is significantly smaller than the other two and the time required to collect adequate data at that peak was prohibitively long. Thus we report data only for the (100) and (200) peaks. As shown in Sec. II, any pair of (*h*00) reflections with *h* even and odd are sufficient to solve the problem of edge separation in BaTiO<sub>3</sub>.

The influence of the anomalous corrections to  $F_j$  on the intensity spectrum can be seen clearly in Figure 2 as the series of cusps at the Ti K and Ba L<sub>III</sub> and L<sub>II</sub> edges. The fine structure contribution is clearly visible in the oscillatory structure above each resonant energy. Due to the  $e^{i\mathbf{Q}\cdot\mathbf{R}_j}$  term in Eq. (1), the Ba and Ti planes scatter in phase in the (200) reflection (or, indeed, for any even order (*h*00) reflection) while they scatter out of phase

for the (100) reflection. This phase relationship is why the cusp at the Ti K edge points upwards in the (100) spectrum and downwards in the (200). As we discuss in Sec. II, we exploit this phase relationship to extract the Ti fine structure  $\chi(k)$ .

## II. ANALYSIS OF THE DAFS DATA

As in earlier work [3,4], we use an iterated Kramers-Kronig technique to isolate the Ti contribution to the spectra shown in Figure 2. Unlike the earlier work, in the present case the resonant atoms are in different crystallographic sites *and* are of different resonant energies. The formalism used to separate the copper site contributions in YBa<sub>2</sub>Cu<sub>3</sub>O<sub>7</sub> [10] was modified to accommodate the different resonant energies. Our analysis procedure is broken into three parts. First, the structure factor of Eq. (1) is fit to the data to obtain initial values for the anomalous scattering function for BaTiO<sub>3</sub>. Second, the solution is iterated to obtain a stable anomalous scattering function. Finally,  $f''(E)$  for the Ti atom is extracted and analyzed using techniques developed for EXAFS.

### A. Initial Fit Using the Structure Factor

In the first step of our data analysis procedure, the data and Eqs. (1) and (2) are used to isolate the real part of the anomalous correction to the scattering factor for the entire crystal. First we optimize the following equation

$$\Delta(E, \mathbf{Q}) = I_m(E, \mathbf{Q}) - P(E, \mathbf{Q}) - A(E, \mathbf{Q}) \left| \sum_j F_j(E, \mathbf{Q}) e^{i\mathbf{Q}\cdot\mathbf{R}_j} M_j \right|^2 \quad (3)$$

where  $I_m(E, \mathbf{Q})$  is the measured intensity for a given reflection  $\mathbf{Q}$ ,  $F_j$  is the full complex scattering factor of Eq. (2),  $M_j$  is the crystallographic Debye-Waller factor, and  $P(E, \mathbf{Q})$  is an empirical polynomial background function. This background function is just a line, as expected from the energy response of the detectors over a small energy range. The difference function  $\Delta(E, \mathbf{Q})$  is evaluated in an energy range from 4920 – 5475 eV. We found that it was difficult to obtain a stable solution in Sec. IIB using an energy range that covered the Ba L<sub>II</sub> edge energy, thus we truncated the fit to the range given. This limited energy range is acceptable as we do not expect the Ti fine-structure spectrum to be measurable at such high energies.  $\Delta(E, \mathbf{Q})$  is minimized by varying several parameters for each reflection. These parameters are the coefficients of the background lines and an overall scaling factor for each reflection. The amplitude function  $A(E, \mathbf{Q})$  includes the scaling factor and such energy dependent corrections to the diffracted intensity as the Lorentz [11] and absorption [12] corrections.

As this experiment measures  $\sigma$ - $\sigma$  scattering, the polarization correction is unity. The energy shift and titanium position parameters are further explained below. In addition, we used two parameters in common to the two reflections — the energy shifts for the  $f'(E)$  and  $f''(E)$  functions from the two atoms. These were refined by performing the fits to the two reflections simultaneously.

To evaluate Eq. (3), initial guesses for the normal and anomalous parts of the scattering amplitudes of the component atoms in BaTiO<sub>3</sub> are required. For the Thomson scattering  $f_j^0(\mathbf{Q})$ , tabulated values [13] are used. For the small anomalous correction to the oxygen scattering, values from the tables [13] of Cromer and Lieberman are used. To obtain a good initial fit to the data and, subsequently, a stable iterative solution to the imaginary part of the anomalous scattering function for the crystal, we found the values from the Cromer–Lieberman tables to be inadequate for Ti and Ba. The Cromer–Lieberman tables neglect solid state effects, such as the white lines observed in Figure 1. Consequently the cusps in the structure factors obtained by using these atomic anomalous corrections were not as sharp as those observed in the data. This results in unstable solutions in the iterative phase of the analysis presented in Sec. II B.

We obtained improved results by constructing approximations to the anomalous scattering corrections for Ti and Ba in BaTiO<sub>3</sub> from the absorption data in Figure 1. Using the recently developed DIFFKK program [14], we construct initial  $f''(E)$  functions for the Ti and Ba atoms by truncating the absorption data, converting it from the absorption function  $\mu(E)$  to  $f''(E)$  by the optical theorem [15], and matching it to the Cromer–Lieberman values of  $f''(E)$  at energies far from the edges. These approximations to the true solid state  $f''(E)$  functions were then Kramers–Kronig transformed using Maclaurin’s formula [16] to produce approximations to the true  $f'(E)$  functions. The results of this procedure are shown in Figure 3 and are inserted into Eq. (3). Energy shifts for each element are used to align the  $f'(E)$  and  $f''(E)$  functions with the data. The edge shifts are optimized along with the other variable parameters when  $\Delta(E, \mathbf{Q})$  from Eq. (3) is minimized. Figure 4 shows the structure factor and background line along with the data from the initial fit to the (100) reflection.

At this stage of the data analysis it would be appropriate also to refine the position of the Ti atom in the unit cell. Although the oscillatory structure in the DAFS data depends only on the local structure, the position in reciprocal space of the measured diffraction peak and the shape of the DAFS spectrum depend on the crystallographic structure of the material measured. At 130 K, bulk BaTiO<sub>3</sub> is rhombohedral and the Ti atom is displaced slightly along all three crystal axes from the nominal perovskite position of  $(\frac{1}{2}, \frac{1}{2}, \frac{1}{2})$ . However, when the  $\Delta(E, \mathbf{Q})$  for the (100) and (200) reflections were minimized with the fractional coordinate of the titanium atom along the axis parallel to the momentum transfer of the diffracted beam as a fitting parameter, we found the value

of this parameter to be ill-defined and highly correlated to the energy shift and background parameters. Consequently, it was fixed to the bulk value of 0.4853 from Ref. [17]. We suspect that, with a larger sampling of diffraction peaks, it would be possible to refine crystallographic information of that sort along with the local structure information we obtain in our analysis.

## B. Iterative Fit to Isolate the Anomalous Scattering for the Entire Crystal

To isolate the anomalous scattering corrections for the entire BaTiO<sub>3</sub> crystal, we use an iterative Kramers–Kronig analysis method that is rigorously correct when a certain symmetry condition is met in the direction of the photon momentum transfer. When the symmetry of the crystal is such that either the  $\cos(\mathbf{Q} \cdot \mathbf{R}_j)$  or the  $\sin(\mathbf{Q} \cdot \mathbf{R}_j)$  term in Eq. (1) vanishes and the squaring of the scattering amplitude yields no terms containing the product of  $f'(E)$  and  $f''(E)$ , then the iterative Kramers–Kronig technique of Refs. [4] and [10] can be applied. One way of satisfying this condition is if the resonant atoms are mirror symmetric about the scattering plane.

In BaTiO<sub>3</sub>, the Ba atom is taken to be at the origin, thus the  $e^{i\mathbf{Q} \cdot \mathbf{R}_j}$  term for Ba is 1 for all  $\mathbf{Q}$ . The Ti atom, however, is slightly displaced from its nominal position at  $(\frac{1}{2}, \frac{1}{2}, \frac{1}{2})$  as shown in the previous section. This slightly breaks the mirror symmetry about the ( $h00$ ) planes, thus the  $e^{i\mathbf{Q} \cdot \mathbf{R}_j}$  term has a small imaginary component for both the (100) and (200) reflections. The full solution of Eq. (1) has terms that are mixed in  $f'(E)$  and  $f''(E)$  and the iterative approach is formally incorrect. Neglecting the small mixed components greatly simplifies the following equations and allows us to apply the iterative solution. The extent to which the introduction of this small error effects the data will be assessed in Sec. II C.

From Eq. (2) let

$$\begin{aligned}\bar{f}'_x(E) &= f'_x(E) + \Delta f''_x(E)\chi'_x(E) \\ \bar{f}''_x(E) &= f''_x(E) + \Delta f'_x(E)\chi''_x(E)\end{aligned}\quad (4)$$

where  $x$  represents either Ba or Ti. We introduce the  $\bar{f}$  notation to distinguish the atomic portion of the anomalous correction from the anomalous correction which is measured in the solid state and which contains  $\chi(E)$ . We express all of the Thomson scattering terms and the small anomalous correction of the oxygen as

$$\begin{aligned}|\mathcal{F}(E, \mathbf{Q})|e^{i\Phi} &= \sum_{\text{all}} f_j^0(\mathbf{Q})e^{i\mathbf{Q} \cdot \mathbf{R}_j} \\ &+ \sum_{\text{oxy}} [f'(E) + if''(E)]e^{i\mathbf{Q} \cdot \mathbf{R}_j}.\end{aligned}\quad (5)$$

Because the thermal factors  $U_j$  in Ref. [17] are small, the  $M_j = e^{-U_j Q^2}$  is close to unity. For simplicity, it will be taken as 1 for the remainder of this discussion. Generalizing to consider non-unity  $M_j$  is a simple extension.

With the approximation of mirror symmetry and the definitions of Eqs. (4) and (5) we can rewrite Eq. (3) as

$$\Delta(E, \mathbf{Q}) = I_m(E, \mathbf{Q}) - P(E, \mathbf{Q}) - |\mathcal{F}|^2 \{ [\cos \Phi + \alpha(E)]^2 + [\sin \Phi + \beta(E)]^2 \} \quad (6)$$

where

$$\alpha(E) = (\bar{f}'_{\text{Ba}} \mp \nu \bar{f}'_{\text{Ti}}) / |\mathcal{F}| \quad (7)$$

$$\beta(E) = (\bar{f}''_{\text{Ba}} \mp \nu \bar{f}''_{\text{Ti}}) / |\mathcal{F}|. \quad (8)$$

The  $-$  or  $+$  signs in  $\alpha$  and  $\beta$  refer to the (100) or (200) reflections respectively. The crystallographic weighting coefficient  $\nu = \sum e^{i\mathbf{Q}\cdot\mathbf{R}_j}$  is close to 1 as the Ti atom is close to the high symmetry  $(\frac{1}{2}, \frac{1}{2}, \frac{1}{2})$  position.

Using the value of  $\beta(E)$  from the initial fit, we solve for  $\alpha(E)$  using Eq. (6) and the value of  $\Phi$ , which is the phase of Eq. (5). At this point the  $\bar{f}$  functions from Ba and Ti are mixed together for each reflection. Because the Kramers–Kronig transform is a linear transform,  $\alpha(E)$  and  $\beta(E)$  are themselves a Kramers–Kronig conjugate pair. Having solved for  $\alpha(E)$ , we can transform using Maclaurin’s formula [16] to obtain a new value for the  $\beta(E)$  function.

Using these newly derived  $\alpha(E)$  and  $\beta(E)$  functions, we again minimize the  $\Delta(E, \mathbf{Q})$  from Eq. (6). This time the parameters that we optimize are the linear coefficients, the overall amplitude  $|\mathcal{F}|^2$ , and a correction to  $\Phi$ . These minimizations are performed independently for each reflection. In all cases, the linear coefficients and amplitudes changed very little from their values from the initial fit and the final value of  $\Phi$  was 5 degrees or less. After minimizing  $\Delta(E, \mathbf{Q})$ , a new value for  $\alpha(E)$  is extracted and Kramers–Kronig transformed to obtain a new value for  $\beta(E)$ . This process is iterated until a stable solution for  $\beta(E)$  is found. Typically this requires about 15 iterations. The final  $\beta(E)$  functions for the (100) and (200) reflections are shown in Figure 5. The different phase relationship of the diffraction from Ti and Ba planes in the (100) and (200) reflections is apparent by the opposite directions of the Ti steps when the Ba step is normalized to +1.

### C. Analysis of Ti Edge Signal

The goal of this analysis procedure is to extract the titanium signal from the (100) and (200) reflections. As suggested by Eq. (8), we add together the  $\beta(E)$  shown in Fig. 5 to isolate  $\bar{f}''_{\text{Ti}}(E)$ . Because we have normalized the  $\beta(E)$  spectra to the size of the Ba edge step, we simply add the spectra with no additional scaling factor. This cancels the Ba contribution to  $\beta(E)$  with needing to know the value of  $\nu$  in Eqs. (7) and (8). The result of this summation is shown in Figure 6 and is the main result of this paper. Although the spectrum in Figure 6 resembles EXAFS data with a large monochromator glitch, it

is certainly analyzable well beyond the Ba edge. The weighting parameter used in combining the spectra is adjusted so that the background function is continuous through the Ba edge energy and the glitch-like feature is minimized.

Because  $\bar{f}''(E)$  is simply related by the optical theorem [15] to the  $\mu(E)$  measured in EXAFS, we can apply the formalism developed to separate  $\chi(k)$  from  $\mu(E)$ . In analogy to the standard separation [2] of  $\chi(k)$  and  $\mu(E)$ , we can write

$$\bar{f}''(E) = f''(E) \cdot [1 + \chi''(E)] \quad (9)$$

where  $f''(E)$  is the atomic portion of  $\bar{f}''(E)$  and is related to the EXAFS  $\mu_0(E)$  by a factor of  $E^{-1}$ . We use the program AUTOBK [18] to extract  $\chi(E)$  from the  $\bar{f}''(E)$  spectrum and to convert the abscissa from energy to photoelectron wave number by the relation  $k = \hbar^{-1} \sqrt{2m(E - E_0)}$ . As stated in Sec. I, we obtained 3 scans at each reflection at 130 K. The analysis outlined in the previous section requires one scan at each reflections. The average  $\chi(k)$  from the 9 possible combinations of data is shown in Figure 7 along with the  $\chi(k)$  spectrum extracted from the EXAFS data in Figure 1.

In the energy range below the Ba  $L_{\text{III}}$  edge, the DAFS experiment must reproduce the EXAFS result. Although,  $\bar{f}''(E)$  and  $\mu(E)$  differ by a factor of  $E^{-1}$ , the two spectra should show the same characteristic near-edge features. The inset to Figure 6 shows the near-edges of  $\bar{f}''(E)$  and  $\mu(E)$ . Although the experimental energy resolution is broader in our DAFS measurement than in the EXAFS measurement, these are comparable spectra. In Figure 7, the  $\chi(k)$  measured by DAFS and EXAFS are compared in the range below the Ba edge, showing excellent agreement. The DAFS and EXAFS measurements agree below the Ba  $L_{\text{III}}$  edge and the titanium displacement is consistent with the bulk value. This suggests that the error introduced by neglecting the lack of mirror symmetry of the Ti atom is small. As the data meet these qualitative consistency checks, we now quantitatively analyze the entire  $\chi(k)$  spectrum.

We removed the large, mostly high frequency feature between 8.25 and 8.7  $\text{\AA}^{-1}$ , as shown in Fig. 8. This feature is due to the incomplete cancellation of the Ba white line, from the  $\chi(k)$  data. It was replaced by a smooth interpolation from the surrounding points. In the EXAFS literature this process is often referred to as “deglitching”. This “glitch” in the  $\chi(k)$  spectrum contributes systematic error to our data at all frequencies and contributes most of the spectral content at high frequencies, which corresponds to the large  $R$  region in  $R$ -space. Removing it has little effect on our fits or on our interpretation of the fits because we apply a band-pass filter to the data by limiting the range of the fit in  $R$ -space [19]. Removing the feature does not remove the systematic uncertainty which it introduces in the frequency range measured, but it does result in  $|\tilde{\chi}(R)|$  spectra which are mostly unaffected by high-frequency ringing.

We analyzed  $\chi(k)$  using the FEFFIT program [19]. FEFFIT performs the fit to the data in  $R$ -space using calculated path contributions from FEFF6 [20] as fitting standards. As the fitting model, we use the rhombohedral crystallographic structure [17] as the basis for the local structural model introduced into FEFFIT. This introduces four structural parameters for the measured local structure. These are the lattice constant, the rhombohedral distortion of the titanium atom, and two parameters determining the position of the oxygen atom. In the fit we included contributions from the first three single scattering shells as well as several multiple scattering paths involving the near neighbor oxygen and titanium atoms. In all, 13 single and multiple scattering paths were used. Along with the four structural parameters, we considered a mean-square displacement  $\sigma^2$  for each scattering shell, three overall phase corrections  $E_0$ , and a passive electron reduction parameter  $S_0^2$ . The procedural parameters used to define the fit are given in Table I.

From the positions of the (100) and (200) peaks, we found a lattice constant of 4.0043(2) Å. This value was then fixed in the fits to  $\chi(k)$ . From previous work [8] on the Ba K edge of BaTiO<sub>3</sub>, the temperature dependence of the Ti–Ba bond was found to be consistent with an Einstein temperature [21] of 267(5) K. Using this value, we fixed the  $\sigma^2$  for the Ti–Ba bond at 0.0027 Å<sup>2</sup>. The fits to these data were found to be insensitive to the parameter describing the displacement of the oxygen atom perpendicular to the direction of momentum transfer. This parameter was fixed at 0.016(8) as found from analysis of the Ba K edge in Ref. [8]. The remaining parameters were varied to produce the fit shown in Fig. 9. The values of these parameters are shown in Table II.

The fit in Fig. 9 is not of exceptionally high quality, which is unsurprising given the large systematic error introduced by the incomplete cancellation of the Ba white line and the large amount of data processing involved in this technique. This error mostly affects the magnitude of the complex Fourier transform. As seen in the bottom panel of Fig. 9, the phase of the transformed data is fit well, particularly in the region of  $R$ -space containing single and multiple scattering at the distance of the third shell Ti atom. The ability to analyze this region of the spectrum is the great benefit of the extended data range afforded by DAFS measurement.

Despite the misfit in Fig. 9, the analysis of this data yields reasonable results with error bars typical of EXAFS analysis. The values for  $S_0^2$  and the  $\sigma^2$ 's are consistent with that for Ti in other Ti containing perovskites [22,23]. Their rather large uncertainties arise from the various sources of systematic uncertainty. The value for  $\Delta z_{Ti}$  is consistent with the value obtained from the Ba K edge fits in Ref. [8]. The value found for  $\Delta z_O$  is consistent with the bulk crystallography value from Ref. [17]. From these results we conclude that, even with the problem at the Ba edge energy, the DAFS technique presented in this paper yields data that is quantitatively analyzable beyond the Ba edge energy.

### III. DISCUSSION

The problem of measuring XAFS in a material with several closely spaced absorption edges can be solved using DAFS. In an EXAFS experiment on such a material, the proximity of the two edges truncates the usable data range at the lower energy absorption edge. In this paper, we have demonstrated that the crystallographic sensitivity of DAFS can be used to isolate the lower energy spectrum, yielding high quality data which can be analyzed using standard EXAFS analysis tools. Using measurements of the (100) and (200) reflections of BaTiO<sub>3</sub>, we isolated and analyzed the Ti fine structure. Several aspects of this work merit further discussion.

Prior knowledge of the crystal structure of BaTiO<sub>3</sub> was used in the data analysis technique presented in Sec. II. The a priori knowledge of the crystal structure may not always be required, however. Much of the structure of the diffracted intensity of Eq. (1) is due to the crystallographic structure of the material and can be refined from the initial fit described in Sec. IIA. Therefore sufficient information can, in principle, be refined from the data to allow the separation of edges even in a material for which the crystallographic structure is not well known.

To obtain stable results in the iterative phase of the data analysis described in Sec. IIB, we found the Cromer-Lieberman tables of  $f'(E)$  and  $f''(E)$  unacceptable. These tables neglect solid state contributions to these functions. Far from the resonant energy of an atom, this is not a serious approximation. However, near the resonant energy, where these functions are changing most rapidly, the tabulated values seriously misrepresent the measured functions [14]. To rectify this in BaTiO<sub>3</sub>, we constructed approximations to the  $f''(E)$  functions from transmission EXAFS data measured on powdered BaTiO<sub>3</sub>.  $f''(E)$  is converted to  $\mu(E)$  using the optical theorem and matched far from the resonant energy to the tabulated atomic values.  $f''(E)$  is then Kramers–Kronig transformed to obtain  $f'(E)$ . We suggest that this approach be considered for all materials to assure a good initial fit and a stable iterative fit.

The extracted  $\bar{f}''(E)$  function is sensitive to the detailed cancellation of the signal from the higher energy edge. In this work, the Ba L<sub>III</sub> white lines did not cancel completely. This is a large source of systematic error in the measurement. To make the signal from the higher energy edge cancel completely, it is essential that high quality data be collected at all reflections. In our experiment, we measured the diffracted signal by measuring the intensity at the top of the peak at each energy. Although it would be a simple application of feedback to track the maximum of the peak, a feedback mechanism of this sort was not available to us at the time of our measurements. An inconsistency in the peak tracking could account in part for the incomplete cancellation of the Ba white line observed in Fig. 6. The integration of the diffracted intensity at each energy point rather than

the measurement of the peak height is another possible improvement to the measurement technique.

As seen in Fig. 2, BaTiO<sub>3</sub> has the interesting property that the diffracted intensity of its (100) reflection nearly vanishes at an energy just above the Ba L<sub>III</sub> edge. Except around that point in the (100) spectrum, the diffracted signal is large compared to the scattered and fluoresced signals. Around that energy, the signal is very sensitive to the measurement details as well as the background and absorption corrections in Eq. (3). Small error either in the measurement or the approximation of the experimental corrections will lead to error in determination of  $\beta(E)$  from Eq. (8). Indeed, we see in Fig. 5 that the Ba L<sub>III</sub> white line is about 6% smaller in the normalized  $\beta(E)$  extracted from the (100) reflection than from the (200) reflection.

Although BaTiO<sub>3</sub> was a successful candidate for the first application of the technique presented here, the relatively large separation of the edges provided one of the challenging aspects of the analysis. The fine-structure signal from the Ti edge is small compared to the size of the Ba edge step. In a material with more closely spaced edges, the relative size of the fine-structure from the lower energy edge may be larger compared to the step of the higher energy edge. The conditions favoring this technique, closely spaced absorption edges and fluorescence lines, are met by many materials combining transition metal and rare earth elements, including a variety of magnetic materials of technological interest. Materials with elements adjacent on the periodic table, assuming those elements lie in different crystallographic sites, and Materials containing transuranic and light metallic elements are also candidates for this technique.

Finally we wish to revisit the possibility of direct measurement of the Ti signal by rejection of the Ba fluorescent line. As stated in the introduction, our attempt to use an energy discriminating Si(Li) detector failed to resolve the two fluorescent lines. The 45 volt separation between the lines was within the resolution of the Si(Li) detector. Our attempt to measure the weaker Ti K <sub>$\beta_1$</sub>  line also failed due to the proximity of the Ba L <sub>$\beta_1$</sub>  line. Finer energy resolution is available with wavelength dispersive detection using an analyzer crystal. A newly developed spectrometer with energy resolution of around 10 eV [24] and with reasonable throughput over a broad energy range has been reported. With the advent of very bright third generation synchrotron sources, it is now reasonable to expect that a measurement using an analyzer crystal could be accomplished on a similar time scale as the DAFS measurement reported here. However, the DAFS measurement is site selective and so is applicable when the element of interest is in multiple crystallographic sites *and* has a fluorescence line near another in the material. We plan in the future to present a comparison between data collected on BaTiO<sub>3</sub> using a wavelength dispersive method and the data presented here.

## ACKNOWLEDGMENTS

We thank A. Carter for providing the BaTiO<sub>3</sub> thin film sample and J. Woicik for help with the Si(Li) detector. We also thank J.O. Cross for inspirational conversation and M. Newville for kindly supplying source code for the differential Kramers-Kronig transform. This work was supported in part by the National Research Council.

- 
- [1] E.A. Stern, W.T. Elam, B.A. Bunker and K. Lu, *Nuc. Inst. Meth.* **195**, 345 (1982).
  - [2] E. A. Stern and S. M. Heald, in *Handbook of Synchrotron Radiation*, edited by E. E. Koch (North-Holland, New York, 1983), Chap. 10, pp. 995–1014.
  - [3] L. Sorensen *et al.*, in *Resonant Anomalous X-ray Scattering: Theory and Applications*, edited by G. Materlik, C. Sparks, and K. Fischer (North Holland, Amsterdam, 1994).
  - [4] I.J. Pickering, M. Sansone, J. Marsch, G.G. George, *Jpn. J. Appl. Phys.* **32 Suppl.** **32-2**, 206 (1993).
  - [5] H. Renevier *et al.*, *Phys. Rev. Lett.* **78**, 2775 (1997).
  - [6] H. Stragier *et al.*, *Phys. Rev. Lett.* **69**, 3064 (1992).
  - [7] J. Vacínová *et al.*, *J. Synchrotron Rad.* **2**, 236 (1995).
  - [8] B. Ravel, E. A. Stern, R. I. Vedrinskii, and V. Kraizman, *Ferroelectrics* **206-207**, 407 (1998).
  - [9] J. L. Ferrer *et al.*, *J. Synchrotron Rad.* **5**, 1346 (1998).
  - [10] J. Cross *et al.*, *J. Phys. IV, Colloq.* **7**, 745 (1997).
  - [11] R. James, *The Optical Principles of the Diffraction of X-Rays* (Ox Bow Press, Woodbridge, CT, 1962), secs. II.2.d and II.2.f.
  - [12] J. Cross, Ph.D. thesis, University of Washington, 1996.
  - [13] S. Brennan and P. Cowan, *Rev. Sci. Instr.* **63**, 850 (1992).
  - [14] J. Cross *et al.*, *Phys. Rev. B* (1998), to be published.
  - [15] B. Cullity, *Elements of X-Ray Diffraction*, 2nd ed. (Addison-Wesley, New York, 1978).
  - [16] K. Ohta and H. Ishida, *Appl. Spectr.* **42**, 952 (1988).
  - [17] G. H. Kwei, A. C. Lawson, S. J. L. Billinge, and S. W. Cheong, *J. Phys. Chem.* **97**, 2368 (1993).
  - [18] M. Newville *et al.*, *Phys. Rev. B* **47**, 14126 (1993).
  - [19] E. A. Stern *et al.*, *Physica B* **208&209**, 117 (1995).
  - [20] S. I. Zabinsky *et al.*, *Phys. Rev. B* **52**, 2995 (1995).
  - [21] E. Sevilano, H. Meuth, and J. Rehr, *Phys. Rev. B* **20**, 4908 (1979).
  - [22] N. Sicron, B. Ravel, Y. Yacoby, E.A. Stern, F. Dogan, and J.J. Rehr, *Phys. Rev. B* **50**, 13168 (1994).
  - [23] B. Ravel, Ph.D. thesis, University of Washington, 1997.
  - [24] M. L. Rivers and S. R. Sutton, *Rev. Sci. Instr.* **66**, 1454 (1995).
  - [25] L. Brillouin, *Science and Information Theory* (Academic Press, New York, 1962).

TABLE I. Parameters used to define the fit using FERFIT. Included in the table are the Fourier transform range in photoelectron wavenumber, the  $k$ -weight used in the transform, the width  $\delta k$  of the symmetric Hanning window sill centered on the ends of the transform range, and the fitting range in  $R$ -space. An approximation to the number of independent data points in the measurement  $N_{idp}$  is calculated using the Nyquist criterion [25]. The number of fitted variables,  $N_{var}$ , is discussed in the text.

| $k$ -range             | $k$ -weight | $\delta k$ | $R$ -range | $N_{idp}$ | $N_{var}$ |
|------------------------|-------------|------------|------------|-----------|-----------|
| 2–10.5 Å <sup>-1</sup> | 1           | 1.5        | 1.1–4 Å    | 17        | 8         |

TABLE II. Results of the fit to  $\chi(k)$  using FERFIT and FERFIT.  $S_0^2$  is the passive electron reduction factor. The  $E_0$ 's are an overall energy shifts for the single scattering paths from FERFIT.  $\sigma_{\text{Ti-O}}^2$  and  $\sigma_{\text{Ti-Ti}}^2$  are the mean square length variations of the Ti–O and Ti–Ti single scattering paths.  $\Delta z_{Ti}$  is the displacements of the Ti atom from a fractional position in the unit cell of  $\frac{1}{2}$  and  $\Delta z_O$  is the fractional displacement of the O atom in that direction.

|   |  |
|---|--|
| $S_0^2 = 0.59(12)$                                      | $E_0(O) = 5.34(83)$ (eV)                                 |
| $E_0(Ba) = 4.13(77)$ (eV)                               | $E_0(Ti) = 1.16(3.05)$ (eV)                              |
| $\sigma_{\text{Ti-O}}^2 = 0.0024(60)$ (Å <sup>2</sup> ) | $\sigma_{\text{Ti-Ti}}^2 = 0.0154(59)$ (Å <sup>2</sup> ) |
| $\Delta z_{Ti} = -0.011(8)$                             | $\Delta z_O = 0.017(8)$                                  |

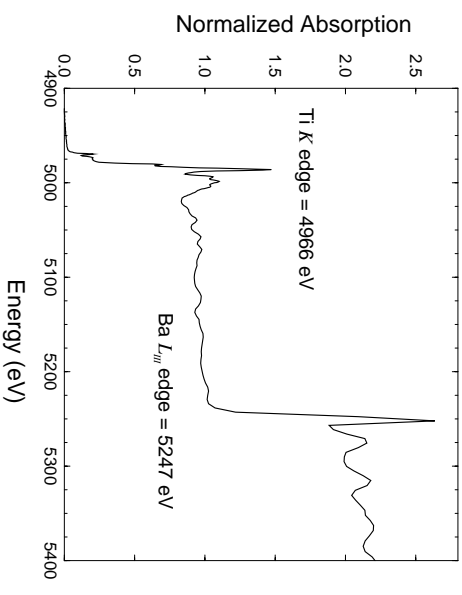


FIG. 1. The Ti K and Ba L<sub>III</sub> edges of BaTiO<sub>3</sub> at 80 K obtained by transmission EXAFS. These data are normalized to a Ti edge step of +1.

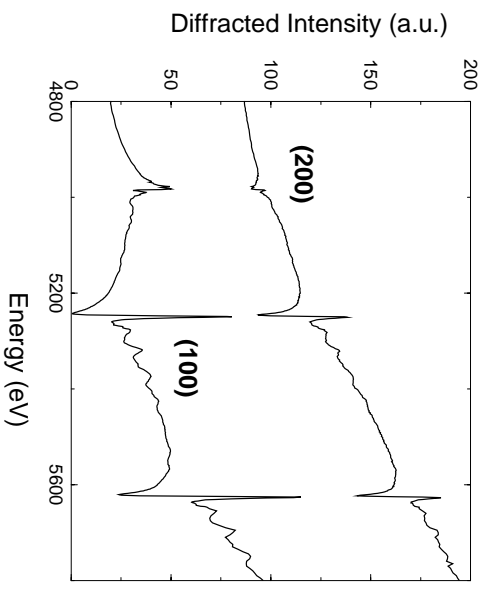


FIG. 2. Measured DAFS spectra of the (100) and (200) reflections from BaTiO<sub>3</sub> at 130 K. The (200) spectrum is displaced upwards for clarity. Note that the anomalous correction to the scattering factor causes the intensity of the (100) peak to diminish at 5244 eV by almost two orders of magnitude relative to its value at the beginning of the data range.

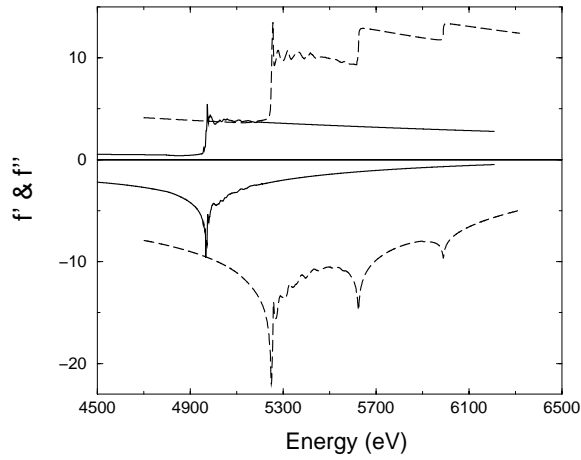


FIG. 3. Approximations to the  $f'(E)$  and  $f''(E)$  functions for Ti (solid lines) and Ba (dashed lines). The  $f''(E)$  were obtained by truncating the data in Figure 1, converting from  $\mu(E)$  to  $f''(E)$ , and matching it to atomic values for  $f''(E)$ . The  $f'(E)$  were then obtained by Kramers-Kronig transform using the DIFFKK program [14]. In this way, we obtain functions that better approximate solid state effects near the resonant energies.

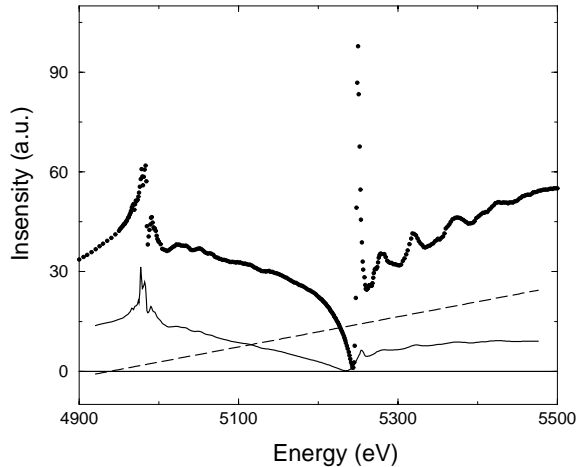


FIG. 4. The results of the initial fit to the (100) data (points) using the  $f'(E)$  and  $f''(E)$  from Figure 3 in the data ranged used in the analysis. The structure factor (solid line) and linear background function (dashed line) are shown along with the 130 K data. The range of the initial fit is given by the extent of the displayed structure factor and background line and does not include the Ba  $L_{II}$  edge. The structure factor and linear background are summed to fit the data, as shown in Eq. (3).

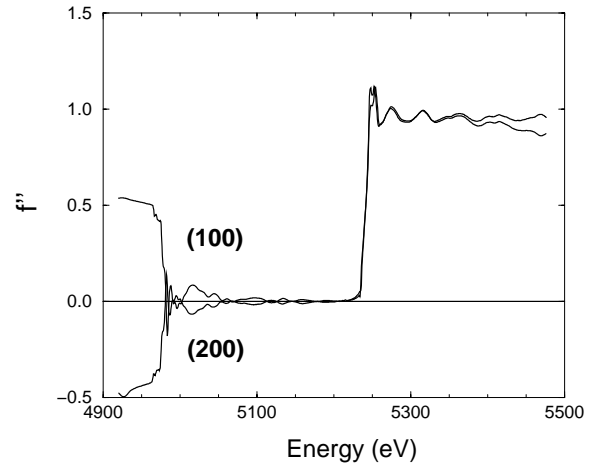


FIG. 5.  $\beta(E)$  from Eq. (8) extracted from the (100) and (200) reflections using the iterated Kramers-Kronig technique. These spectra have been aligned and normalized such that the Ba edge step is +1.

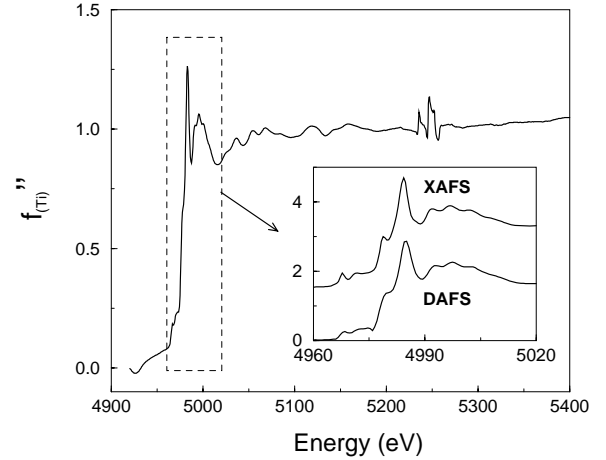


FIG. 6. Extracted  $f''(E)$  for the Ti atom. Note that the Ba edge white line does not cancel completely. The effect of this on the analysis of the Ti  $\chi(k)$  is discussed in the text. The inset shows the near edge region of this spectrum and of the spectrum from Figure 1. Commonly normalized, the EXAFS  $\mu(E)$  and DAFS  $f''(E)$  differ only by a factor of  $\frac{1}{E}$ , thus show the same near-edge structure. The energy resolution of the DAFS measurement is broader than that of the EXAFS measurement.

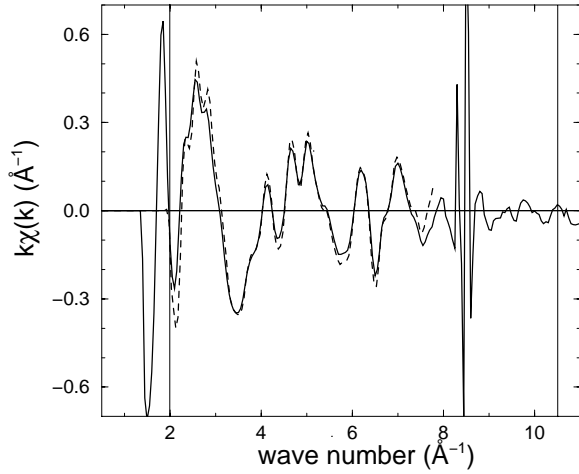


FIG. 7. Extracted  $\chi(k)$  for the Ti atom (solid line). Although the incomplete cancellation of the Ba white line results in the large feature around  $8.2 \text{ \AA}^{-1}$ , the titanium signal clearly extends well beyond that point. The DAFS  $\chi(k)$  is compared to the EXAFS  $\chi(k)$  (dashed line) in the region below the Ba edge. The vertical lines indicate the range in which this data will be analyzed using FEFFIT [19].

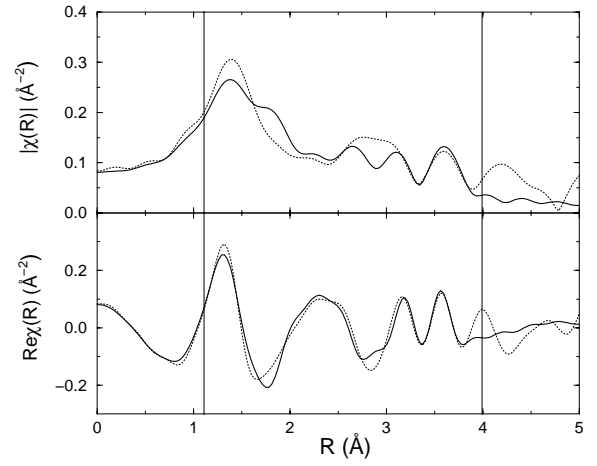


FIG. 9.  $\tilde{\chi}(R)$  (dotted line) compared to the best fit (solid line) using FEFF [20] and FEFFIT [19]. The top panel shows the magnitude of the complex Fourier transform of the  $\chi(k)$  function shown in Fig. 8, the bottom panel shows the its real part. The vertical lines indicate the fitting range. These data are the Fourier transform of the “deglitched” data shown in Fig. 8.

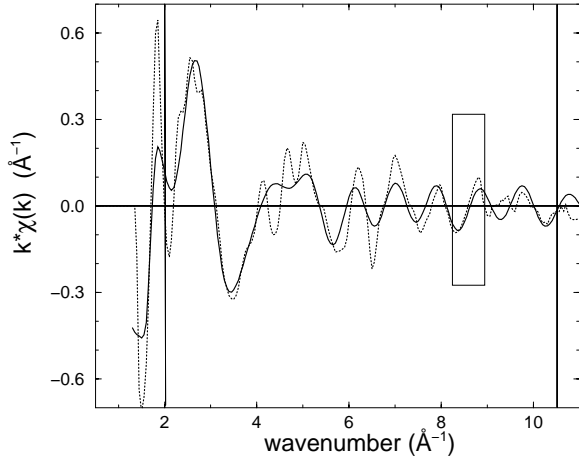


FIG. 8.  $\chi(k)$  extracted from the DAFS data (dotted line) compared to the best fit (solid line) using FEFF [20] and FEFFIT [19]. The box indicates the region from which points were removed from the  $\chi(k)$  data and replaced by a smooth interpolation from the surrounding data. Removing these points does not effect the low frequency spectral content of the signal, but reduces the high frequency ringing in the Fourier transform. The vertical lines indicate the Fourier transform range of the data used in the fit.